Proceedings of the 21st ICSMGE, Vienna, Austria, 14 – 19 June 2026. Pistrol, Adam & Schweiger (eds.)
Published by: ÖGG, Austrian Society for Geomechanics, Salzburg, Austria, ISBN 978-3-9503898-4-5
https://doi.org/10.53243/ICSMGE2026-896

Influence of preconsolidation methods and end restraints on the rate dependent behaviour of reconstituted kaolin specimens in undrained triaxial compression

Kenny Kataoka Sørensen
Department of Civil and Architectural Engineering, Aarhus University, Denmark, kks@cae.au.dk

Sabine Gehring and Hans Henning Stutz
Institute of Soil Mechanics and Rock Mechanics, Karlsruhe Institute of Technology, Germany

ABSTRACT: Previous research has highlighted that preconsolidation procedures and end-restraints in triaxial testing can significantly affect the mechanical behaviour of tested soils. However, the impact on viscous (rate-dependent) behaviour remains largely unexplored, particularly for reconstituted fine-grained soils. This study systematically investigates how sample preparation and boundary conditions affect the rate-dependent shearing behaviour of reconstituted kaolin (medium plasticity silt). The specimens were prepared from slurry and preconsolidated in tubes with diameter ratios of 1.0, 1.4 or 2.6 relative to the initial specimen size and subsequently tested in triaxial compression with step changes in strain rate. Tests used specimen height-to-diameter ratios of 1 (with smooth ends) or 2 (with rough ends), and the influence of top cap fixation was explored. Findings reveal that all specimens exhibited isotach viscous behaviour with rate sensitivity parameters (β) ranging from 5.1 to 6.0, corresponding to approximately 3 % increase in shear strength per 10-fold increase in strain rate. While sample preparation method had minimal effect on rate sensitivity, specimens with fixed top caps showed reduced rate sensitivity ($\beta = 5.1$) compared to free-rotation conditions ($\beta = 5.6 - 6.0$). The study demonstrates that boundary conditions can influence both the mechanical and viscous behaviour of fine-grained soils, providing insights for interpretation and standardisation of triaxial testing of fine-grained soils.

KEYWORDS: Triaxial testing, fine-grained soil, kaolin, strain rate effects, sample preparation, boundary conditions.

1 INTRODUCTION

Test results from laboratory tests do not depend solely on the tested material or soil sample. The test procedure can also significantly affect the obtained results. Factors influencing the results of triaxial compression tests include the sample size, the preparation method, and the type of end-restraints. Despite early discussions on testing methods and variations (e.g., Olsen et al., 1964) and subsequent standardization efforts, different procedures are still used within the geotechnical community, as demonstrated in this study. Several studies in the past and in current research have investigated the influence of slenderness (height-to-diameter $\frac{H}{D}$) ratio and end-restraints. Peri et al. (2019) reviewed many of them and found that most show that a lower $\frac{H}{D}$ ratio is associated with higher strength parameters, while smooth end platens tend to result in lower friction angle. The volume and strain changes at failure are greater for samples with $\frac{H}{D} = 1$ and smooth end platens. These conditions are also related to a more homogeneous stress and strain distribution. Still, some studies report contradictory findings or only a minor influence of $\frac{H}{D}$ ratio and end-restraint variations.

Sample preparation is another factor influencing the results of triaxial tests (Sørensen, 2007, Li et al., 2021). Even when solely using preconsolidated samples from a slurry, various methods are available for sample preparation. Wichtmann & Triantafyllidis (2018) investigated the homogeneity of preconsolidated kaolin in a cylinder with a diameter 2.6 times that of the test specimen. They observed variations in water content near the cylinder wall and the top, outside the region used for the final sample. These variations can be explained by induced friction at the cylinder wall.

The mentioned studies primarily focus on monotonic triaxial tests conducted at a constant deformation rate, leaving the effect of sample geometry, end-restraints and sample preparation on viscous behaviour of fine-grained soil unaddressed. Simultaneously, strain-rate-dependent behaviour itself remains of significant interest and practical relevance.

Many natural fine-grained soils exhibit rate effects consistent with isotach viscosity behaviour (Šuklje, 1957), where unique stress-strain curves correspond to specific strain rates. This behaviour has been widely documented in both 1D compression (e.g. Leroueil et al., 1985) and undrained triaxial tests (e.g. Graham et al., 1983, Sorensen et al. 2007). However, recent studies show that alterations in the natural structure of fine-grained soil through reconstitution can lead to transient rate effects, where persistent strain rate effects are significant only at small strains and diminish near peak strength in triaxial shearing, while temporary rate effects increasingly dominate the behaviour at increasing strains (e.g. Sorensen et al. 2007, 2023). Contradictory findings exist for kaolin specifically, with Tatsuoka et al. (2002) reporting isotach behaviour for normally consolidated pure kaolin in undrained triaxial compression, while Li and Baudet (2016) found transient rate effects in both drained and undrained triaxial compression.

Given these discrepancies, both in the rate-dependent response of kaolin and the influence of $\frac{H}{D}$ ratio and end-restraint, there is a clear need for further investigation. This study aims to clarify these effects through a systematic evaluation of the rate-dependent shearing behaviour of kaolin in undrained triaxial compression under controlled variations in specimen geometry and boundary conditions.

2 TEST MATERIAL AND METHODS

2.1 *Classification properties of Kaolin K1*

The test material used in this study is a commercially available kaolin powder (product name: Kaolin K1), supplied by Gebrüder Dorfner GmbH & Co. Kaolin- und Kristallquarzsand-Werke KG. According to Wichtmann and Triantafyllidis (2018), it classifies as a medium-plasticity silt with a clay-size fraction ($< 2\,\mu m$) of approximately 35% (see grain size distribution in Figure 1a). The material has a liquid limit $w_L = 47\,\%$, plasticity index $I_P = 12\,\%$ and grain density $\rho_s = 2.675\,\frac{g}{cm^3}$.

Scanning Electron Microscope (SEM) imaging reveals a microfabric composed of aggregated stacks of kaolinite

platelets (Figure 1b), which is characteristic of kaolinitic fine-grained soil.

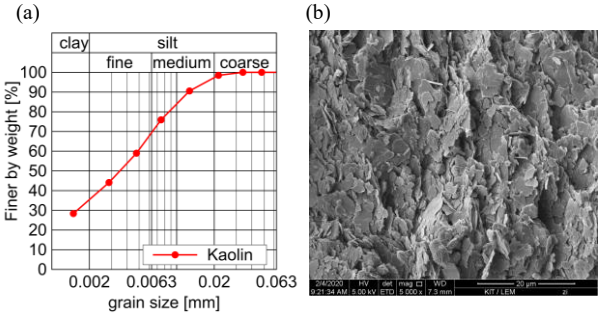

Figure 1. a) Grain size distribution and b) SEM image showing microfabric

2.2 *Sample preparation and specimen dimensions*

Kaolin powder was mixed with deionised water to create a slurry at a water content equal to twice the liquid limit (i.e. $w = 2 \times w_L = 94\,\%$). Samples were preconsolidated in acrylic consolidometers to a nominal vertical effective stress of 200 kPa. Assuming minimal sidewall friction and a lateral earth pressure coefficient $K_0 \approx 0.6$, the nominal mean effective stress during preconsolidation was approximately 145 kPa. The average consolidation stress is however expected to be somewhat lower due to frictional resistance, particularly in consolidometers with smaller diameters.

The following specific preparation methods were used:

- **Method A**: Slurry consolidation in a 70 mm diameter floating ring consolidometer, step-loaded in five stages. Samples were trimmed using a soil lathe to 50 mm in diameter and ends were trimmed in a split mould.
- **Method B**: Similar procedure using a 50 mm diameter floating ring consolidometer, however with no subsequent circumference trimming.
- **Method C**: Consolidation in a 130 mm fixed-ring consolidometer. Samples were directly pressed into a 50 mm diameter mould, and the ends were trimmed.

2.3 *Test apparatus and end platens*

Specimens were tested using the triaxial apparatus - load frame type with internal load cell (setup I, II and IV) or external load cell (setup III) and external displacement measurement and control. Specimens were set up using four different end platen conditions and two different slenderness ratios $\frac{H}{D} = 1$ or 2:

- **Setup I**: Smooth end platens, free rotation of top cap, $\frac{H}{D} = 1$. Filter stone, double layer circular membrane discs (with silicone grease between) with a central 1 cm hole and spiral-cut filter paper were placed against the specimen.

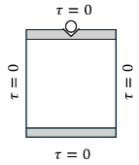

- **Setup II**: Smooth end platens, fixed rotation, $\frac{H}{D} = 1$. Like setup I, apart from the top cap being restrained from rotation using a suction cap.

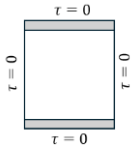

- **Setup III**: Smooth end platens, limited rotation of top cap allowed, $\frac{H}{D} = 1$. End platens were used with a 5 mm central filter stone and 6 mm filter paper applied, the platen was greased and a circular membrane disc with a central hole was placed against the specimen. The end platens were enlarged compared to the specimen diameter to allow for maintenance of full specimen contact during compression stages.

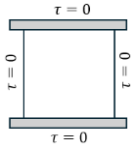

- **Setup IV**: Rough end platens, free rotation of top cap, $\frac{H}{D} = 2$ (standard setup according to DS/ISO 17892-9:2018), filter stone and filter paper were applied directly to the specimen ends.

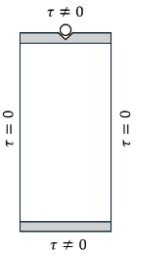

All specimens were isotropically consolidated with drainage permitted only at the specimen top. Pore pressure was monitored at the base.

An overview of the performed tests and combinations of sample preparation methods, $\frac{H}{D}$ ratio and end platen setup are given in 1.

Table 1. Overview of performed tests and test conditions

Test #	Sample preparation method	Setup	$\frac{H}{D}$ ratio	End platen conditions
A1	A	I	1	Smooth/free rotation
A2	A	I	1	"
A3	A	I	1	"
A4	A	II	1	Smooth/fixed rotation
B1	B	IV	2	Rough/free rotation
B2	B	IV	2	"
C1	C	III	1	Smooth/limited rotation
C3	C	III	1	"

2.4 Test procedure and data corrections

Saturation was achieved using a backpressure of 500 kPa and an initial mean effective stress $p' = \frac{1}{3}(\sigma_v' + 2\sigma_h') = 20$ kPa. The resulting B-values ranged from 0.97 to 1.0. Following saturation, specimens underwent incremental isotropic consolidation in four steps ($p' = 50$, 100, 200, 400 kPa) to a final isotropic consolidation stress, $p_c' = 400$ kPa. Undrained shearing was then performed up to 20–25% deviatoric strain, defined as $\varepsilon_s = \frac{2}{3}(\varepsilon_a - \varepsilon_r)$, using stepwise increases in shear strain rate $\dot{\varepsilon}_s$ = [0.001, 0.005, 0.01] %/min. In Test A1, these rates were doubled to [0.002, 0.01, 0.02] %/min. For undrained tests, $\varepsilon_s = \varepsilon_a$ holds.

A uniform cross-sectional area correction was applied during both consolidation and shearing, and a membrane correction was applied to both vertical and horizontal stresses according to DS/ISO 17892-9:2018. Corrections were approximately 2 kPa for horizontal stress and 10 kPa for vertical stress at the failure state. Axial strains recorded during saturation in Test A4 were insignificant ($\varepsilon_a < 0.3\,\%$) hence, both axial and volumetric strains during saturation can be assumed negligible. The void ratio e_c after isotropic consolidation to $p' = 400$ kPa and during subsequent undrained shearing is determined from the final water content of the test specimen under assumption of full saturation. The void ratio after saturation e_0 and during consolidation stages are back calculated from e_c and the measured volume changes on the backpressure line.

3 RESULTS

An overview of the state variables obtained at the start of consolidation, end of consolidation and failure state during undrained shearing (reference rate of 0.01 %/min) are given in Table 2.

Table 2. State variables and parameters for test specimens.

Test #	e_0	e_c	q_{peak}[a]	ε_{peak}	$\frac{q}{p'}_{max}$	φ'_{cs}
	[-]	[-]	[kPa]	[%]	[-]	[°]
A1	1.26	1.01	195	14.9	0.87	22
A2	1.24	1.00	192	10.4	0.86	22
A3	1.26	0.98	193	13.3	0.78	20
A4	1.28	0.99	182	10.7	0.81	21
B1	1.32	1.03	183	13.5	0.81	21
B2	1.31	1.02	186	9.4	0.79	20
C1	1.30	1.03	196	12.6	0.95	24
C3	1.28	1.02	206	12.1	0.95	24

3.1 *Isotropic compression*

Despite different sample preparation methods and end platen conditions the isotropic compression curves are very similar, and similar gradients are obtained in the normal consolidated stress range for $p' > 200$ kPa as seen in Figure 2.

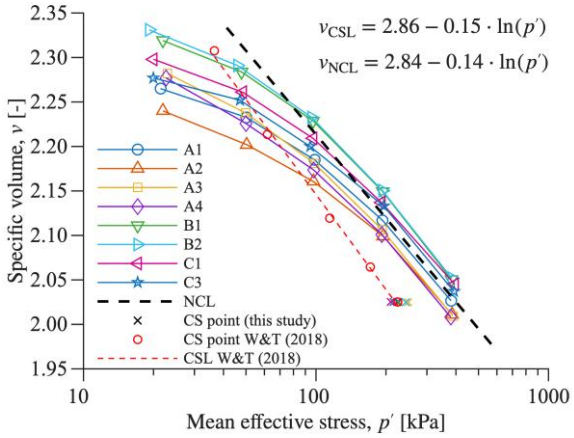

Figure 2. Isotropic compression curves, normal compression line (NCL) and critical state line (CSL)

Consistent grouping of the compression curves is observed which seem linked to the sample preparation method and imposed differences in the soil structure, as further explained in section 3.2 Nevertheless, the differences in final void ratio are small and within ± 0.03 from a common Normal Compression Line (NCL). The NCL is found as the best-fit log-linear regression line to the datapoints at end of consolidation (Casagrandes method) from all tests for $p' \geq 200$ kPa:

$$v_{NCL} = N_p - \lambda \times \ln p' = 2.84 - 0.14 \times \ln p' \quad (1)$$

It is usual to assume that Critical State (CS) coincide with the peak strength state for the normally consolidated specimens (as seen from the stress-strain response and limited evolution of pore water pressure, cf. Figure 5). Hence, the CS points in volumetric space can be determined from the mean effective stress p'_{peak} at the peak deviator stress states in combination with a specific volume which for simplicity is here found based on the common NCL and an applied consolidation pressure $p'_c = 400$ kPa. Additional CS points for specimens of Kaolin K1 normally consolidated to different pressures between 50 kPa and 400 kPa and sheared undrained are added from Wichtmann and Triantafyllidis (2018). A best-fit critical state line (CSL) through the literature CS data points is given by:

$$v_{CSL} = N_0 - \lambda \times \ln p' = 2.86 - 0.15 \times \ln p' \quad (2)$$

As shown later, Wichtmann and Triantafyllidis (2018) found the CSL for kaolin K1 to be non-linear in stress space. This explains why the gradient of the CSL in $v - p'$ space is shown to deviate and be slightly higher than the gradient of the NCL.

3.2 *Qualitative assessment of macro-structure*

After triaxial testing, all specimens (except C1) were split in half (prior to oven drying) to qualitatively examine their macrostructure and assess the effects of preconsolidation, isotropic consolidation, and shearing. Representative photos of the split specimens prepared in 50 and 70 mm consolidometers are shown in Figures 3a-e. Unfortunately, it has not yet been possible to obtain good quality photos of split specimens initially prepared in 130 mm consolidometers; only external photos of the specimens after testing has been obtained, cf. example in Figure 3f.

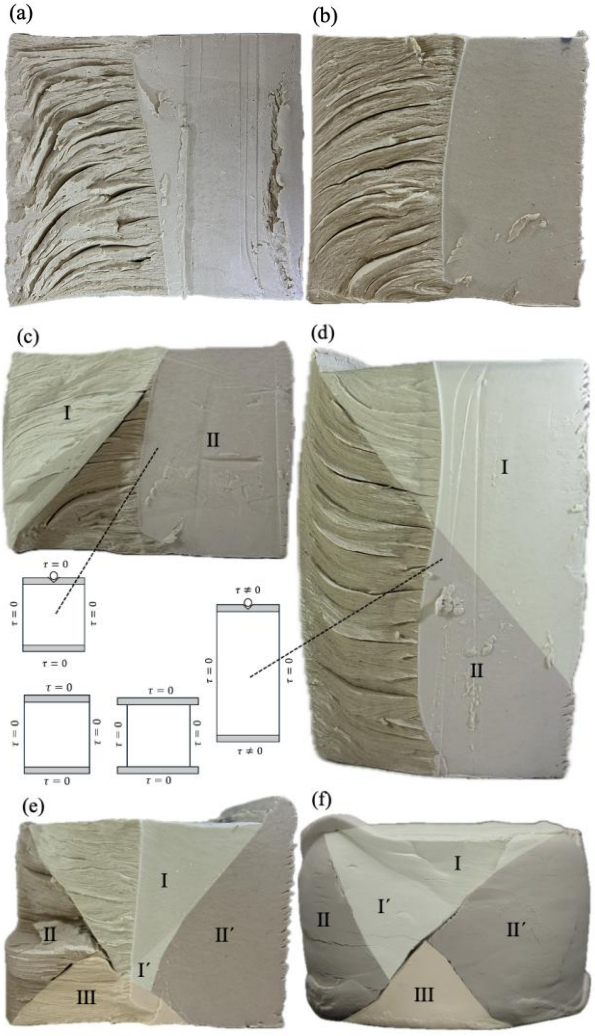

Figure 3. Photo of split sample after a) preconsolidation and trimming (sample preparation method A), b) isotropic consolidation to around $p' = 400$ kPa, and after undrained shearing c) $\frac{H}{D} = 1$ with free smooth top cap (A1), d) $\frac{H}{D} = 2$ with free rough top cap (B1), e) $\frac{H}{D} = 1$ with fixed smooth top cap (A4), and f) external photo of specimen $\frac{H}{D} = 1$ with semi-fixed enlarged smooth top cap (C1)

Distinct layering is evident both after preconsolidation, isotropic consolidation and following undrained shearing in the triaxial cell. Structural features remaining after preconsolidation are clearly visible in all photos. Notably, side friction developed against the 50 and 70 mm acrylic consolidometers causes an increasing rotation of the layers near the specimen boundaries. However, initial observations indicate that the influence of side friction can be minimized when trimming samples from 130 mm to 50mm.

It is furthermore observed that the layers also show signs of separation, which may introduce errors when estimating specimen volume post-testing based on external dimension measurements. However, it is uncertain if this is a result of the sample splitting. CT-scanning is needed to cast light on this.

The failure mode is found to be strongly influenced by end restraints. When the top cap is allowed to rotate freely, the failure mode is seen to be characterised by a single shear band (Figures 3c and 3d), regardless of the specimen's height-to-diameter ($\frac{H}{D}$) ratio. In contrast, top cap fixation is seen to lead to a more symmetrical failure pattern with multiple failure planes as observed in test A4 and C1 (Figures 3e and 3f). The experimental observations are supported by numerical simulations (Kiriyama, 2016).

In addition, specimens with $\frac{H}{D} = 2$ and rough ends display slightly more bulging compared to those with $\frac{H}{D} = 1$ and smooth ends, though this is not very pronounced. From a theoretical point of view, it can be expected that reduced end friction will promote a more uniform strain distribution prior to failure. Nevertheless, all specimens show clear strain localization at failure.

In all the tests, where split photos have been taken, the dominant failure plane consistently forms at an inclination of approximately 50 degrees. For test C1, where only external photos were taken after testing the inclination of the dominant failure plane is harder to assess. It is noted that increased friction from rough end platens does not appear to have a significant effect on the orientation of the failure plane.

3.3 *Isotach stress-strain-rate shearing behaviour*

The $(q - \varepsilon_s)$ stress-strain curves and $(q - p')$ stress paths obtained from the performed tests are shown in Figure 4 and Figure 6 respectively. The results are presented in subplots where they have been grouped based on the applied test setup. The monitored evolution of excess pore water pressure u_e is seen in Figure 5.

The critical state line (CSL) obtained by Wichtmann and Triantafyllidis (2018) in undrained triaxial compression tests on Kaolin K1 using similar sample preparation and test setup to test C1 for $p'_c = 50$ to 400 kPa is added to the $q - p'$ plots (Figures 6a-c). Note that the CSL was found to be non-linear.

All specimens are found to exhibit ductile behaviour as commonly seen from normally consolidated samples. Excess pore pressures are positive, and peak strength is mobilised at high shear strains around 10-15 %. The use of the use of smooth end platens is not found to lead to greater failure strains and reduced softening, as could otherwise be expected if a more uniform strain field was obtained. Instead, significant strain softening is observed in all tests after reaching peak strength, which is clearly linked to the observed strain localization and generation of single or multiple shear bands. Excess pore pressures are seen to stabilize around peak strength, and the peak state can be assumed to coincide with critical state.

All tests show clear isotach stress-strain behaviour in both the pre-peak and post-peak regions. Only tests B1 ($\frac{H}{D} = 2$) and A2 ($\frac{H}{D} = 1$) show evidence of transient effects of rate changes, however this is limited to the steepest portions of the softening curve in the post-peak region. These effects are likely caused by strain localization and the associated significant localized changes to the microstructure and possibly pore pressure evolution as well. The results suggest a slight rate dependence of the pore pressure response. The excess pore pressure is found to increase marginally more per unit shear strain during the slowest shearing stages. However, the stress paths are clearly rate dependent throughout shearing, from initiation up to stresses near the peak. The undrained peak strength is indicated to correlate with the maximum $\frac{q}{p'}$ ratio (directly linked to the critical state angle of friction φ'_{cs}). Although the peak deviator stress exhibits a clear rate dependence, it remains unclear whether φ'_{cs} is independent of strain rate as found by Li and Baudet (2016).

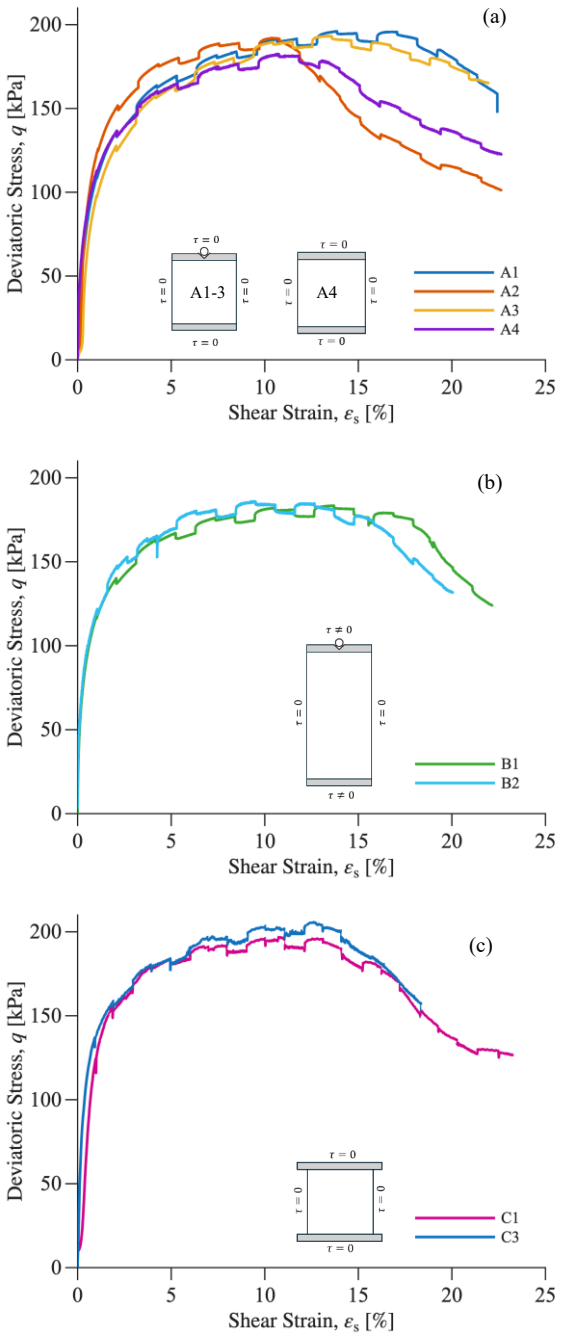

Figure 4. Stress-strain curves a) setup I & II: $\frac{H}{D} = 1$ smooth, b) setup IV: $\frac{H}{D} = 2$ rough, c) setup III: $\frac{H}{D} = 1$ smooth

The results indicate no direct link between the failure mode and the undrained peak strength or φ'_{cs}. Furthermore, the results show minimal influence of slenderness ratio and end restraints (comparing tests A1-4 with B1-2). Yet, test performed with enlarged (and smooth) end platens (test C1 and C3 and additional tests performed by Wichtmann and Triantafyllidis, 2018) clearly show greater undrained peak strength or φ'_{cs} compared to the rest of the tests. This is believed to be a result of the differences in the sample preparation methods which affects the soil structure rather than the differences in the end platens. However, this requires further testing to verify.

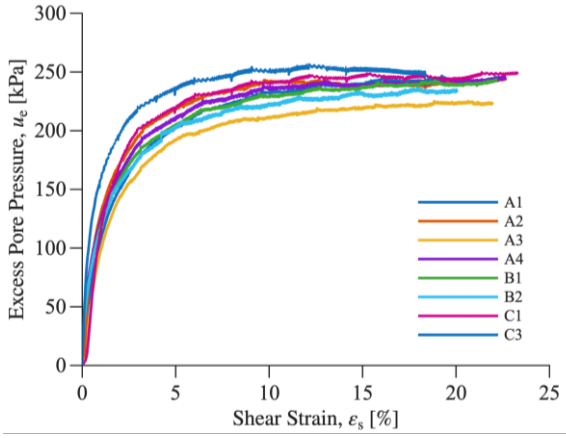

Figure 5. Evolution of excess pore water pressure

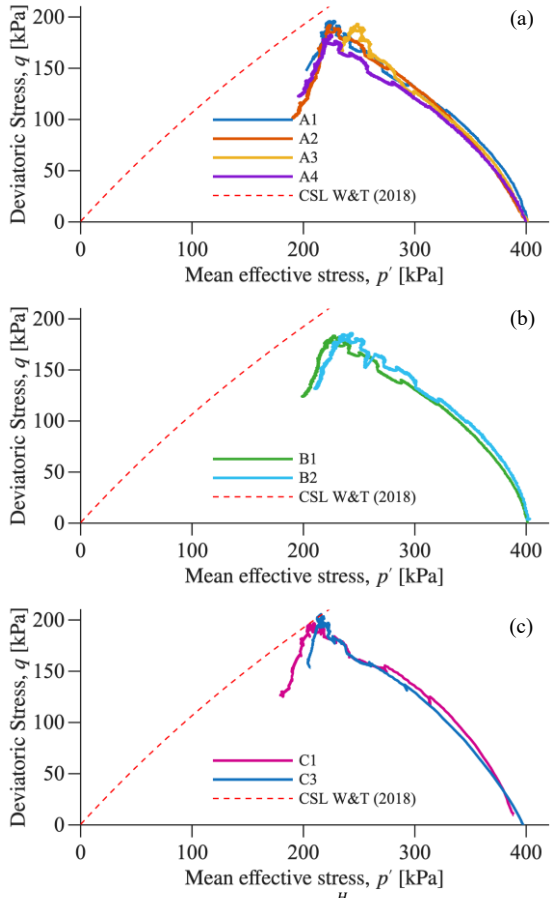

Figure 6. Stress paths a) setup I & II: $\frac{H}{D} = 1$ smooth, b) setup IV: $\frac{H}{D} = 2$ rough, c) setup III: $\frac{H}{D} = 1$ smooth

The strain rate dependent relationship between deviator stress, q and deviatoric shear strain, ε_s at a given strain rate $\dot{\varepsilon}_s$ can be found based on a known reference curve determined at a given reference strain rate $\dot{\varepsilon}_{s,ref}$ using equation (3):

$$q(\varepsilon_s)_{\dot{\varepsilon}_s} = q_{ref}(\varepsilon_s) + \Delta q\left(R_{\dot{\varepsilon}_s}\right) \quad (3)$$

Where q_{ref} is the reference deviatoric stress at the same strain level and $\Delta q\left(R_{\dot{\varepsilon}_s}\right)$ is the additional viscous contribution to the shearing resistance from the change in strain rate by the ratio $R_{\dot{\varepsilon}_s} = \frac{\dot{\varepsilon}_s}{\dot{\varepsilon}_{s,ref}}$. The results of the conducted tests support that the rate effects can be quantified within the applied stress ranges as the jump in deviatoric stress found from the intersection between a constant vertical ε_s line and the extrapolated $q(\varepsilon_s)_{\dot{\varepsilon}_s}$ curve (hyperbolic fit applied) at the new strain rate (see Figure 7).

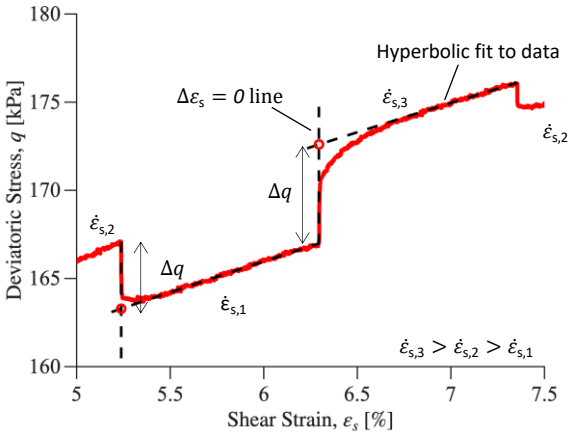

Figure 7. Interpretation of stress jump upon changes in axial strain rate

The results indicate a log-linear relationship between Δq and $R_{\dot{\varepsilon}_s}$, as plotted in Figure 8 and in general terms given by equation (4):

$$\Delta q\left(R_{\dot{\varepsilon}_s}\right) = \beta \times \log R_{\dot{\varepsilon}_s} \quad (4)$$

Where β is the rate parameter. It should be noted that the rate parameter is formulated to be independent of stress level, which fit the data well within the applied stress range. It can be seen from Figure 8 and the listed values of β in Table 3 that the rate sensitivity as quantified by β is very similar for all conducted tests. Nevertheless, the two specimens (A4 and C1), which showed more complex failure patterns with multiple failure lines resulting from a fixed or semi-fixed top cap, interestingly display rate sensitivities which are lower than the rest. The listed β values generally correspond to around 3 % increase in q for a 10-fold increase in strain rate over the given stress range for which strain rates changes were applied.

Table 3. Rate parameters.

Test #	A1	A2	A3	A4	B1	B2	C1	C3
β	5.9	5.6	6.0	5.1	5.8	5.6	5.1	5.7
R^{2*}	0.98	0.98	0.98	0.96	0.98	0.96	0.87	0.96

* coefficient of determination

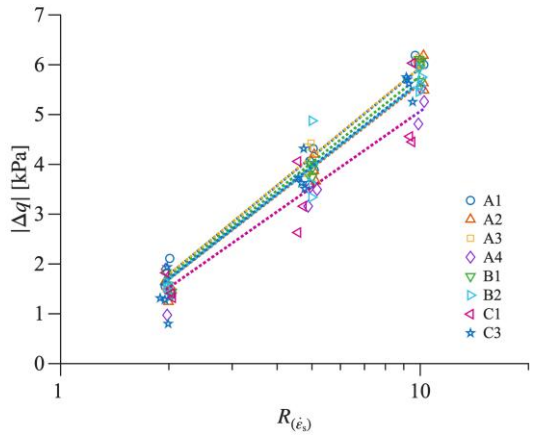

Figure 8. Quantification of stress jump resulting from rate changes

The representative normalized stress-strain curve for specimen A4, shown in Figure 9, demonstrates that normalization with respect to a reference shear rate (0.01 %/min in this case) is effective up to the point of failure, producing a unique normalized stress-strain response. In the post-peak region, the behaviour remains isotach; however, stress jumps caused by rate changes deviate slightly and are somewhat smaller than those observed in the pre-peak region. These deviations lead to minor observed rate effects on the normalized curves in the post-peak region. Further quantification of post-peak rate effects was not within the scope of this study.

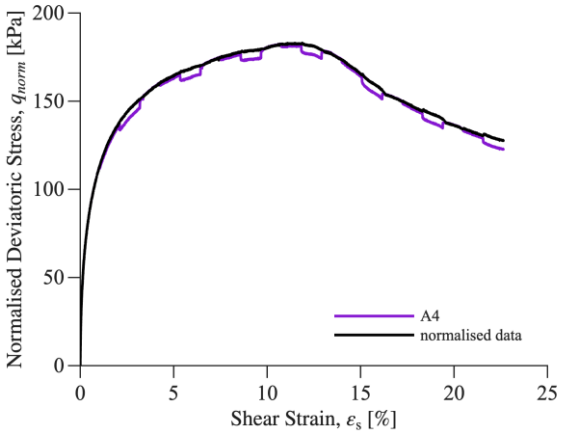

Figure 9. Normalised stress-strain curve – example test A4

4 CONCLUSIONS

This systematic investigation of rate-dependent behaviour in reconstituted Kaolin K1 under varying sample preparation and boundary conditions provides several key insights for both fundamental understanding and testing practice.

Viscous behaviour characterisation: All reconstituted samples displayed clear and consistent isotach behaviour throughout undrained shearing, from pre-peak through post-peak regions after isotropic consolidation to normally consolidated state. The rate sensitivity parameter β ranged from 5.1 to 6.0 across all test conditions, corresponding to approximately 3% increase in shear strength per 10-fold increase in strain rate. This consistency demonstrates that reconstituted kaolin exhibits reliable rate-dependent behaviour that can be quantified using the isotach framework.

Influence of testing configuration and sample preparation: The results show minimal influence of slenderness ratio and end restraints on the undrained shear strength and critical state friction angle. However, the results indicate that the soil structure is influenced by the sample preparation method and side friction during preconsolidation, which in turn can have a measurable effect on the mobilised strength in triaxial compression tests. This requires further testing to study.

Boundary effects on rate sensitivity and failure mode: While slenderness ratio and end platen roughness had negligible impact on rate sensitivity, top cap fixation was found to affect the failure mode and impact the viscous response. Localisation of strains during shearing was observed in all tests. A single shear band developed in all tests when the top cap was not restrained. In contrast, fixation of the top cap was found to promote a more symmetrical failure mode dominated by multiple failure lines and furthermore resulted in reduced rate sensitivity compared to free-rotation conditions. This finding indicates that boundary constraints influence not only failure mechanisms but also fundamental rate-dependent behaviour.

Implications for testing standards: The findings contribute to better interpretation of rate-dependent behaviour in fine-grained soils and inform development of standardized testing procedures for viscous and mechanical characterization.

REFERENCES

Graham, J., Crooks, J. H. A., and Bell, A. L. 1983. Time effects on the stress-strain behaviour of natural soft clays. *Géotechnique*, 33(3), 327-340.

Kiriyama, T. 2016. Numerical study of shear band formation in triaxial compression tests. The 15th Asian Regional Conference on Soil Mechanics and Geotechnical Engineering. 679-702.

Leroueil, S., Kabbaj, M., Tavenas, F., and Bouchard, R. 1985. Stress–strain–strain rate relation for the compressibility of sensitive natural clays. Géotechnique, 35(2), 159-180.

Li, P. Q. and Baudet, B. A. 2016. Strain rate dependence of the critical state line of reconstituted clays. Géotechnique Letters, 6, 66-71.

Li, DQ., Wang, J. and Rui, R. 2021. Effects of specimen preparation method and strain rate on the mechanical responses of a clayey loess. *Arabian Journal of Geosciences,* 14(2550). https://doi.org/10.1007/s12517-021-08879-2

Olson, R. E., Campbell, L. M., Lee, K. L., Seed, H. B., Turnbull, J. M., and Poulos, S. J. 1964. Discussion of "Importance of Free Ends in Triaxial Testing". *Journal of the Soil Mechanics and Foundations Division*, *90*(6), 167-179.

Peri, E., Ibsen, L. B., and Nielsen, B. V. N. 2019. Influence of sample slenderness and boundary conditions in triaxial test – a review. In: E. Ibraim, & A. Tarantino (Eds.), *7th International Symposium on Deformation Characteristics of Geomaterials.* Glasgow.

Sorensen, K. K., Baudet, B. A. and Simpson, B. 2007. Influence of structure on the time-dependent behaviour of a stiff sedimentary clay. Géotechnique, 57 (1), 113–124. https://doi.org/10.1680/geot.2007.57.1.113

Sørensen, K. K., Nielsen, V. K. H., Mikkelsen, A. R., and Stutz, H. H. 2023. Characterization of the rate-dependent behavior of a high-plasticity stiff sedimentary clay. *Geotechnical Testing Journal*, 46(6). https://doi.org/10.1520/GTJ20230339

Suklje, L. 1957. The analysis of the consolidation process by the isotaches method. *In: Proceedings of the International Conference on Soil Mechanics and Foundation Engineering.* 200-206.

Tatsuoka, F., Ishihara, M., DI, B. H., and Kuwano, R. 2002. Time-dependent shear deformation characteristics of geomaterials and their simulation. *Soils and foundations*, 42(2), 103-129.

Wichtmann, T. and Triantafyllidis, T. 2018. Monotonic and cyclic tests on kaolin: a database for the development, calibration and verification of constitutive models for cohesive soils with focus to cyclic loading. *Acta Geotechnica*, 13, 1103-1128.